LHCb/2004–047 TRIG
LPHE/2004–06
July 13, 2004

# Decision Tracks in Minimum-Bias Events Selected by the Level-1 Trigger

**Luis Fernández*** and **Thomas Schietinger†**

Laboratory for High-Energy Physics (LPHE)
Swiss Federal Institute of Technology Lausanne (EPFL)

**Abstract**

We present a systematic analysis of minimum-bias events passing the Level-1 trigger. Various sources of fake and real tracks that can trigger the Level-1 decision are identified and their respective frequencies determined. The analysis is based on the trigger algorithms and data used for the TDR performance studies of 2003.

*Luis.Fernandez@epfl.ch
†Thomas.Schietinger@cern.ch

# Contents

# 1 Introduction

The LHC bunch crossing rate is 40 MHz, including about 10 MHz of crossings with visible proton-proton interactions. The trigger system is designed to reduce this rate down to a few hundred Hertz, rate at which the events will be transferred to final storage and made available for further offline physics analyses. A detailed description of the LHCb trigger can be found in the LHCb trigger system TDR [1].

The Level-0 trigger will reduce the event rate to 1 MHz, based on calorimeter and muon chamber information, whereas the Level-1 stage will achieve a rate reduction from 1 MHz to 40 kHz, thus retaining 4% of the Level-0 accepted minimum-bias events. The Level-1 trigger stage is implemented in software and uses information from the Level-0 decision unit, the silicon vertex locator (VELO) and the trigger tracker (TT) situated before the magnet.

The Level-1 decision algorithm [2] consists of two parts, namely a generic algorithm based on typical $b$-hadron signatures and a set of specific algorithms (or *bonus* system) which enhances the efficiency of some benchmark channels using Level-0 information. This study only addresses the generic part of the algorithm, which fills up about 30 kHz or 75% of the Level-1 bandwidth.

The first typical signature of $b$-hadron decays used in this generic part is that secondary vertices are significantly displaced with respect to the production vertex, due to the long lifetime of $b$-hadrons. These detached secondary vertices will yield tracks with high impact parameter with respect to the corresponding primary vertex. The second feature exploited by the generic trigger is the presence of tracks with high transverse momentum with respect to the beam axis, as a consequence of the large $b$-hadron mass.

The trigger strategy of the generic Level-1 algorithm thus exploits the above two features as typical signatures of a $b$-event by requiring two tracks (the so-called *decision tracks*) with these properties in order to reduce the background originating from light quark flavor states. The impact parameters are obtained using the VELO information whereas the determination of the transverse momenta is based on the extrapolation of VELO tracks to the TT stations ("VELO to TT matching") where the residual magnetic field is sufficient to estimate the momenta [3, 4].

The aim of this study is to understand why minimum-bias events can trigger at Level-1. In particular we aim at identifying the most frequent causes for false triggers in order to provide some guidance to future efforts at improving the Level-1 trigger. Since the Level-1 decision is, in the case of the generic algorithm, triggered by two high $p_T$ tracks, we will classify these decision tracks with respect to the various possible sources of error, such as bad $p_T$ resolution, wrong VELO to TT matching, wrong impact parameter assignment due to the presence of several primary vertices, etc.

The software and data used for this study are described in Sec. 2. In Sec. 3, the physics particles and decays that give rise to decision tracks are identified by use of the Monte Carlo truth. We investigate the various mechanisms producing tracks with high $p_T$ and high impact parameter in Secs. 4 and 5, respectively, before summarizing our findings in Sec. 6.

## 2 Data and software

This analysis is based on the trigger algorithms and data used for the TDR performance studies of 2003 [1, 5].

We start from the sample of so-called stripped minimum-bias events (TriggerFilter v2r1) which contains 10533 events passing both Level-0 and Level-1 triggers. Using a newer software version we apply a recalibrated Level-1 threshold corresponding to 40 kHz output rate, which leaves us with a sample of 7191 events. The data sample used to determine the recalibrated Level-1 global threshold $\Delta_{0.04}$ consists of 494000 events of event type 61 (minimum-bias), yielding $\Delta_{0.04} = -0.154523$. Among the 7191 events in our sample, 5220 are triggered by the generic algorithm. In other words, 1971 events – representing 27% of the bandwidth – trigger due to one of the specific algorithms (bonus system).

The Level-1 algorithms used are those of the L1Decision v2r2 package and were run in DaVinci v9r1. For the detailed investigation of VELO to TT matching, information on the TT clusters is needed. Since the Monte Carlo (MC) relations for the L1 clusters were not stored during the stripping, we use *offline* TT clusters; the matching performance is assumed to be identical [6]. Also, to retrieve the MC truth information on the decision tracks, the L1FixVeloTrack2MCAlg associator is used. Finally, note that the Level-0 information is available to the Level-1 trigger through the Level-0 Decision Unit (L0DU); this information will be needed when discussing the effect of the Pile-Up system in Sec. 5.

## 3 Origin of the decision tracks

Using the MC truth information, we can determine the origin of the two 3D Level-1 tracks with highest transverse momentum (denoted by $p_{T1}$ and $p_{T2}$) that triggered a given minimum-bias event according to the Level-1 trigger generic algorithm (i.e. with no bonus). These two tracks are referred to as decision tracks.

Figure 1 shows that the decision tracks mainly originate from light resonances, which predominantly decay to pions and kaons. Another sizable set of tracks consists of tracks originating from direct charged particles such as pions or kaons. These tracks in general have (MC-) true vanishing impact parameters as they are pointing back to the primary vertex. Non-zero impact parameters are, however, possible due to multiple scattering.

We further see that Level-1 does trigger on tracks coming from $b$-hadrons, which is of course our goal. Note that there is an open charm component among the decision tracks as well. One expects to trigger on this kind of events since they share the features exploited in the Level-1 trigger for the decays of interest, namely high $p_T$ tracks and the presence of detached secondary vertices.

Figure 1 suggests the definition of the following four *truth* categories[1] which will be used later for the classification of tracks according to their source of high-$p_T$:

*A* tracks from light resonances: $\rho$, $\omega(782)$, $K^*$, $\phi(1020)$;

[1]The charge conjugate states are implicitly included.

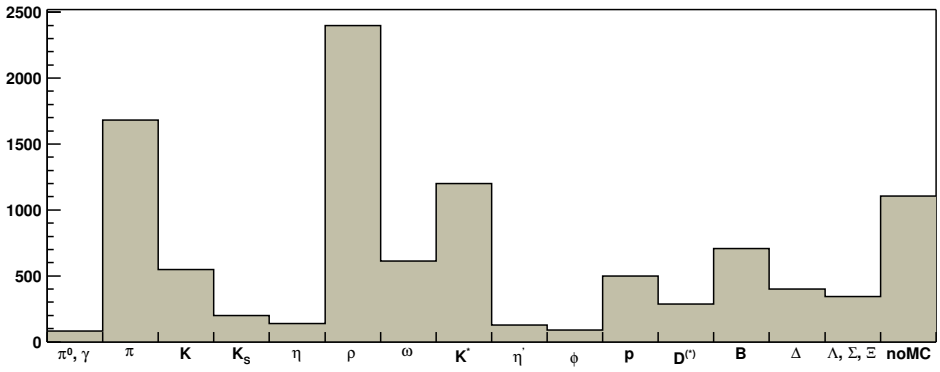


**Figure** 1: Origin of the Level-1 decision tracks.

$B$ tracks from $b$-hadrons: $B_d^0$, $B_u^+$, $B_s^0$, $B_c^+$, $\Lambda_b^0$;

$C$ direct charged tracks, i.e. mainly $\pi$, $K$, $p$ (technically defined as tracks that have an MC association whose C++ pointer to the mother particle is NULL);

$R$ remaining tracks (including a charm component: $D$, $D^*(2010)$, $D_s^*$, $\Lambda_c$).

The separation of categories $A$ and $C$ is motivated by the different momentum spectra of the two (see also Sec. 4.2).

Table 1 lists the fraction of each category, excluding the 1106 tracks for which no MC association was found (10.6 $\pm$ 0.3)% of all decision tracks). The charm component of category $R$ represents (3.1 $\pm$ 0.2)% of all the associated tracks.

**Table** 1: Fractions of the different truth categories. The uncertainties are statistical.

| Category | $N_{\rm tr}$ | Fraction [%] |
|---|---|---|
| $A$ | 4300 | 46.0 $\pm$ 0.5 |
| $B$ | 761 | 8.2 $\pm$ 0.3 |
| $C$ | 2695 | 28.9 $\pm$ 0.5 |
| $R$ | 1578 | 16.9 $\pm$ 0.4 |
| Total number of associated tracks: 9334 | | |

# 4 Decision tracks: why they have high $p_T$

In this Section we will try to classify the decision tracks according to the reason for them being assigned high $p_T$. The two principal sources for high $p_T$ tracks are tracks with true high $p_T$ and low $p_T$ tracks that are assigned high $p_T$ by error. Among the latter class, we may distinguish VELO tracks which are correctly matched to TT (but are assigned a high $p_T$ due to resolution effects) and tracks that are matched to the wrong hits in TT (and thus are assigned some arbitrary $p_T$).

Both distinctions, well versus badly measured $p_T$ as well as correct versus wrongly matched tracks, are arbitrary to some degree. In order to proceed with our quantitative analysis of decision tracks, we need to find definitions for both. We first define the notion of wrong TT matching in the following Subsection. Based on this definition we may then address the question of good and bad $p_T$ measurement in Subsection 4.2.

Note that there is a fourth category of decision tracks, namely tracks with no measured $p_T$ at all. In the TDR version of the Level-1 trigger algorithm, tracks with no $p_T$ measurement are assigned the average $p_T$ of 400 MeV/$c$, and may become decision tracks, provided that there is not more than one track with measured $p_T$ higher than 400 MeV/$c$. Clearly, in a triggered event sample, we will find these tracks only as sub-leading decision tracks ($p_{T2}$), given the high effective $p_T$ threshold of Level-1.

## 4.1 Definition of correct and wrong TT matching

The Level-1 momentum determination is based on the VELO to TT matching, which combines the Level-1 3D VELO tracks with hits in the TT stations. A TT hit is said to be correct if it is associated to a TT cluster and if this cluster in turn corresponds to a TT cluster used for the VELO to TT matching.

If we define the correct hit ratio as being the ratio of the number of correct TT hits to the number of TT cluster used for the VELO-TT matching, we have the following list of values for the possible ratios:

$$0,\ 1/4,\ 1/3,\ 1/2,\ 2/3,\ 3/4,\ 4/5,\ 1\,.$$

Figure 2 shows us the distribution of the correct TT hit ratio. In particular, we see that we have basically either no correct TT hits at all (bin at zero) or perfect TT matching (ratio equal to 1).

The adopted definition for correct TT matching is such that the track has at least 75% of correct TT hits, allowing in this way for a possible mistake in the VELO to TT matching. The choice of this definition is justified by comparing the $p_T$ resolutions for the different ratios. Also, asking for 75% of correct TT hits implicitly requires to have at least three correct TT hits, which corresponds to the requirement of having at least three TT hits with acceptable $\chi^2$ from the least-squares fit of the VELO–TT matching [1, 3].

With the above definition of correct and wrong matches we can determine the composition of the $2 \times 5220 = 10440$ decision tracks and their corresponding frac-

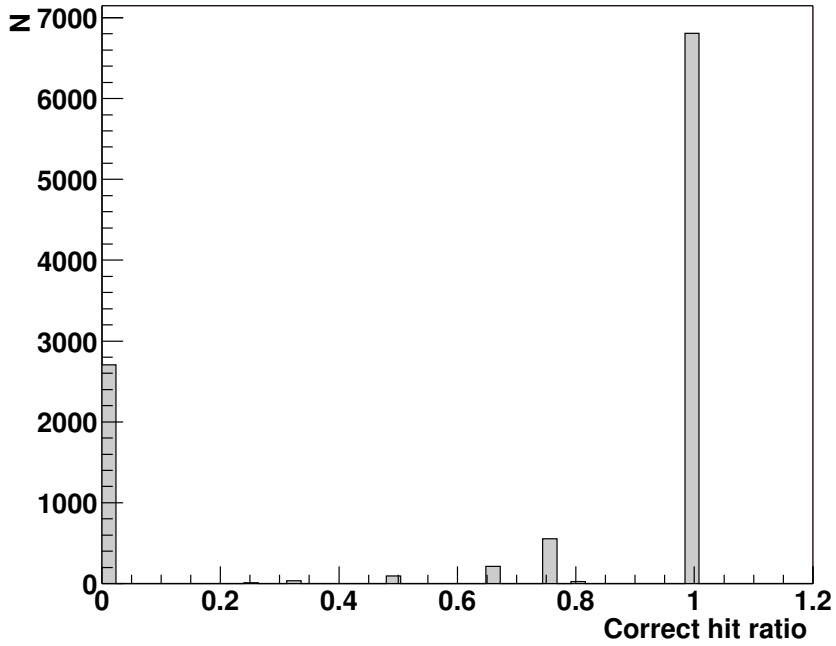


**Figure** 2: Correct TT hit ratio distribution.

tions, see Table 2. We observe that the sample is dominated by tracks that are correctly matched to TT. As we can further read off this table, there is no apparent difference between the two decision tracks; we will henceforth consider both decision tracks together.

**Table** 2: Composition of the 10440 decision tracks with respect to VELO–TT reconstruction. The uncertainties are statistical.

| Track type | $N_{p_{T1}}$ | $F_1$ [%] | $N_{p_{T2}}$ | $F_2$ [%] | Total | $F_{\text{tot.}}$ [%] |
|---|---|---|---|---|---|---|
| Correct TT | 3752 | 71.9 ± 0.6 | 3630 | 69.5 ± 0.6 | 7382 | 70.7 ± 0.4 |
| Wrong TT | 747 | 14.3 ± 0.5 | 457 | 8.8 ± 0.4 | 1204 | 11.5 ± 0.3 |
| Not hitting TT | 97 | 1.9 ± 0.2 | 55 | 1.1 ± 0.1 | 152 | 1.5 ± 0.1 |
| No MC asso. | 624 | 11.9 ± 0.4 | 482 | 9.2 ± 0.4 | 1106 | 10.6 ± 0.3 |
| MC asso., no $p_T$ | 0 | 0.0 ± 0.0 | 596 | 11.4 ± 0.4 | 596 | 5.7 ± 0.2 |

## 4.2 Definition of good and bad $p_T$ measurement

The decision whether the $p_T$ measurement of a given track should be considered good or bad, i.e. whether the assigned (high) $p_T$ is sufficiently close to the track's

true $p_T$ for the purpose at hand (triggering on $b$-hadrons) is a priori arbitrary. To arrive at a quantitative assessment, we may consider the following quantity:

$$r \equiv \frac{\log(p_T^{\rm rec}) - \log(p_T^{\rm mc})}{\log(p_T^{\rm mc})} \lessgtr q \ , \tag{1}$$

i.e., the relative logarithmic deviation $r$ of the measured $p_T^{\rm rec}$ from the true $p_T^{\rm mc}$, and require that it be below some quality criterion $q$. Figure 3 shows the integrated distributions of correctly and wrongly matched decision tracks as a function of the quality criterion $q$, thus providing us with a visualization of the $p_T$ resolutions involved.

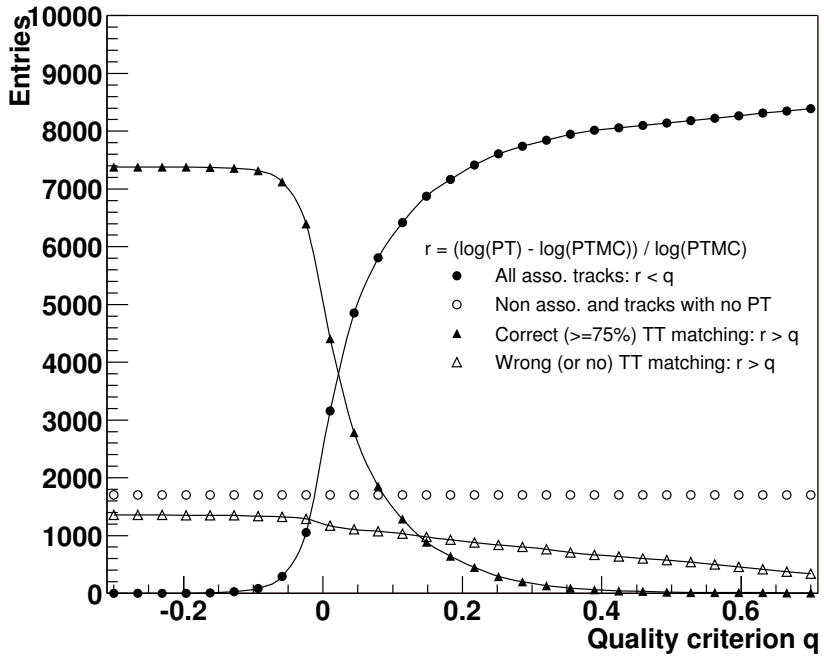


**Figure** 3: Integrated distribution of the decision tracks as a function of the $p_T$ quality criterion $q$.

Among the correctly matched tracks, we may compare the same resolution curves for the truth categories introduced in Sec. 3, see Fig. 4. We see from this plot that the relative falloff is faster for the truth category $B$ compared to the other categories, meaning that the decision tracks originating from $b$-hadron decays have a better measured $p_T$. This plot thus suggests the following definition for $q$:

- define $q$ such that we retain 95% of the correctly matched $b$-hadron tracks; this corresponds to a logarithmic limit in $p_T$ resolution of $q = 11.1\%$.

In Sec. 3, we introduced the truth categories making a distinction between tracks from light resonances (category $A$) and direct tracks (category $C$). This distinction

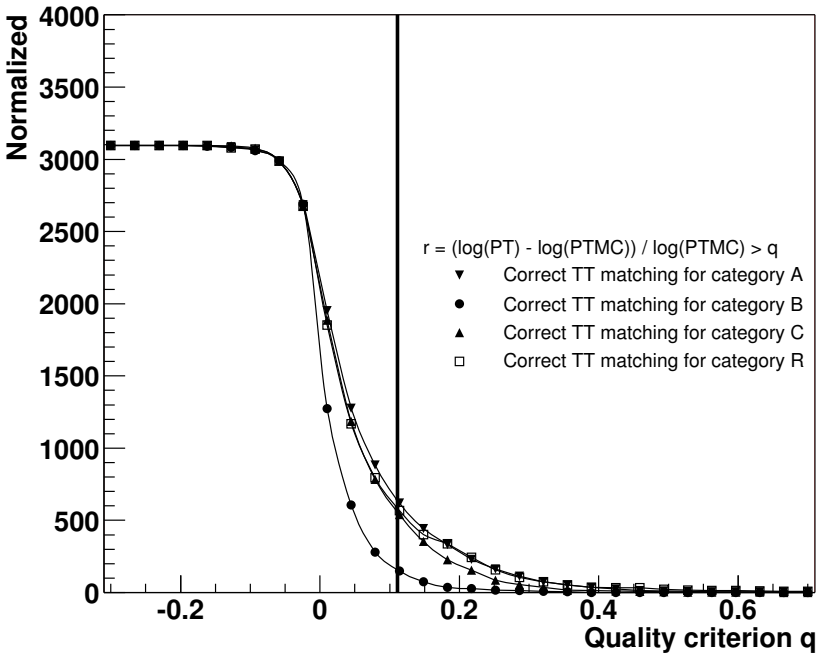


**Figure** 4: Integrated distribution of the decision tracks with correct TT matching as a function of the $p_T$ quality criterion $q$, normalized to the same total.

is motivated by the fact that tracks belonging to the category $A$ have on average a lower true momentum ($\langle p \rangle = 4.9\,\mathrm{GeV}/c$) compared to the tracks of category $C$ ($\langle p \rangle = 8.3\,\mathrm{GeV}/c$). Since the VELO–TT reconstruction is based on the distance of TT hits to a VELO straight line extrapolation passing the four layers of TT [3, 4], low momentum tracks will have a larger curvature inside TT therefore leading to a higher probability for wrong TT matches. This effect is illustrated in Fig. 5.

## 4.3 $p_T$ categories

We summarize the categories used to classify decision tracks according to $p_T$:

- The decision track has a true high transverse momentum if $r \leq q$:
  - **Good $\mathbf{p_T}$** category: the track has a well reconstructed $p_T$;
- The decision track has a false high transverse momentum if $r > q$:
  - **Bad $\mathbf{p_T}$** category: the track is correctly matched to TT but has a badly reconstructed $p_T$ due to momentum resolution;
  - **Wrong $\mathbf{p_T}$** category: the track is wrongly or not matched to TT;

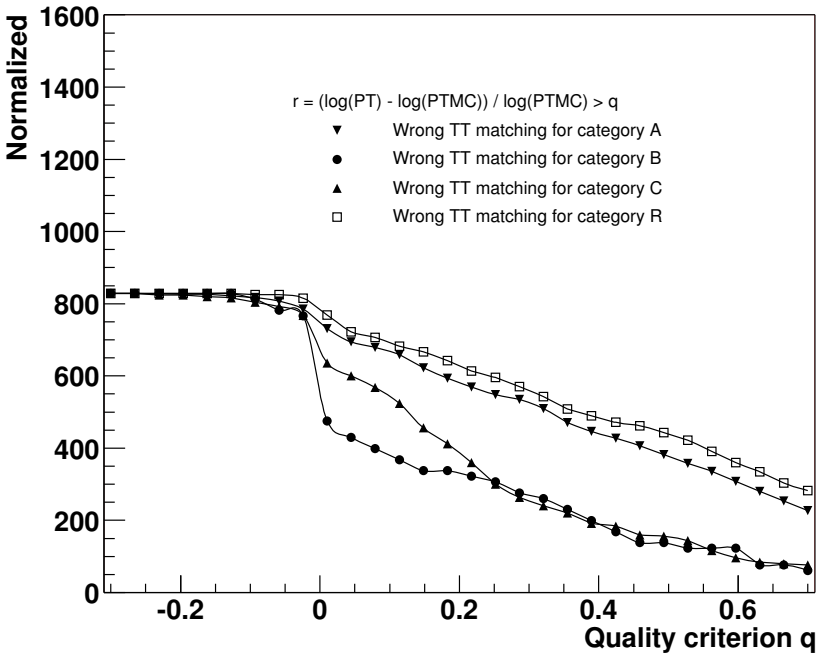


**Figure** 5: Integrated distribution of the decision tracks with wrong TT matching as a function of the $p_T$ quality criterion $q$, normalized to the same total.

– **Else** category: the track has no MC association or no assigned $p_T$.[2]

## 4.4 Decision tracks breakdown according to $p_T$

Using the definitions of the previous Subsection, we obtain the breakdown of the decision tracks in the Level-1 triggered minimum-bias sample shown in Table 3 and Fig. 6. The sample is clearly dominated by the good $p_T$ category, which means that most of the triggers are justified from the point of view of $p_T$ determination.

Also given in Table 3 are the compositions of the various $p_T$ categories in terms of the truth categories defined in Sec. 3. We see that $b$-hadron tracks (category $B$) represent 11% of the good $p_T$ tracks, but less than 3% of each of the bad and wrong $p_T$ categories. Conversely, we find that 92% of all $b$-hadron tracks end up in the good $p_T$ category, consistent with our definition of good $p_T$ and a small fraction of wrong matches. We further observe that the fraction of tracks that acquire high-$p_T$ due to bad momentum resolution does not vary much between the background categories $A$, $C$, and $R$, consistent with the picture given by Fig. 4.

In Fig. 7 we give the $p_T$ spectra for the three $p_T$ categories. The distributions of both the bad $p_T$ and the wrong $p_T$ tracks exhibit large tails resulting in high values for the mean $p_T$.

[2]Tracks with no assigned $p_T$ (due to TT reconstruction failure) are assigned $p_T = 400\,\mathrm{MeV}/c$ in the Level-1 algorithm.

**Table** 3: Number of decision tracks $N$ in each of the $p_T$ categories, and further split into the truth categories of Sec. 3. The fractions $F$ in the "All" row are normalized to all tracks, the fractions given for the truth categories $A$, $B$, $C$, and $R$ are normalized to the respective $p_T$ categories. The uncertainties are statistical.

| True | Good $p_T$ | | Bad $p_T$ | | Wrong $p_T$ | | Else | |
|---|---|---|---|---|---|---|---|---|
| Cat. | $N$ | $F$ [%] | $N$ | $F$ [%] | $N$ | $F$ [%] | $N$ | $F$ [%] |
| All | 6376 | $61.1 \pm 0.5$ | 1324 | $12.7 \pm 0.3$ | 1038 | $9.9 \pm 0.3$ | 1702 | $16.3 \pm 0.4$ |
| $A$ | 2627 | $41.2 \pm 0.6$ | 637 | $48.1 \pm 1.4$ | 660 | $63.6 \pm 1.5$ | - | - |
| $B$ | 699 | $11.0 \pm 0.4$ | 35 | $2.7 \pm 0.4$ | 25 | $2.4 \pm 0.5$ | - | - |
| $C$ | 2061 | $32.3 \pm 0.6$ | 437 | $33.0 \pm 1.3$ | 133 | $12.8 \pm 1.0$ | - | - |
| $R$ | 989 | $15.5 \pm 0.5$ | 215 | $16.2 \pm 1.0$ | 220 | $21.2 \pm 1.3$ | - | - |

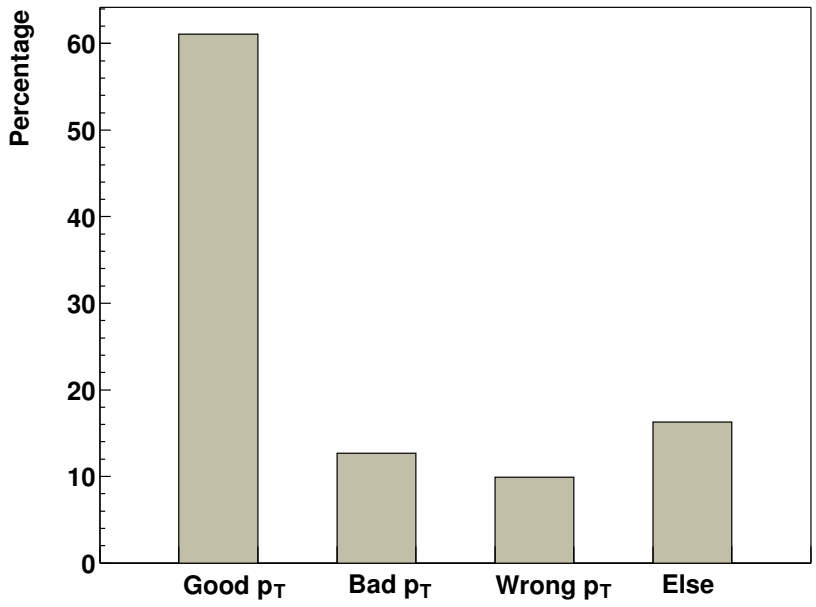


**Figure** 6: Graphical representation of the composition of the 10440 decision tracks according to the cause for high-$p_T$.

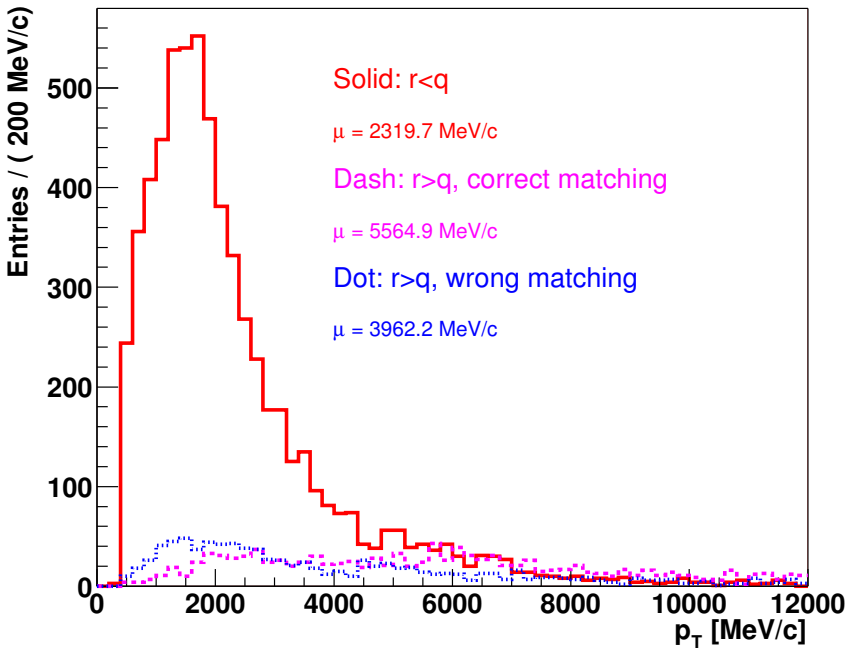


**Figure** 7: Reconstructed $p_T$ of the decision tracks.

# 5 Decision tracks: why they have large impact parameter

Besides exploiting the high transverse momentum feature as a signature of a $b$-hadron track, the generic part of the Level-1 strategy also uses the fact that $b$-hadrons are long-lived particles. This property translates at the track level to the presence of tracks with high impact parameter (IP) with respect to the production vertex.

In the Level-1 algorithm, the IP selection criterion is applied before the tracks are extrapolated to TT for the measurement of $p_T$, first after the 2D reconstruction, then confirmed in 3D. Only tracks with IP between 0.15 and 3.0 mm with respect to the primary vertex are kept for the $p_T$ measurement.

In the last Section, we have seen that for the large majority of tracks the assignment of high-$p_T$ is indeed correct, and the positive trigger decision therefore justified for what concerns $p_T$ only. Yet, we have also seen that only 11% of these tracks actually arise from decays of $b$-hadrons. A fraction of comparable size originates from charm decays, but the large remainder of more than 70% is due to light resonances and primary tracks. Clearly, these tracks should have a very small impact parameters if any, and therefore have been eliminated by the IP requirement.

The question why these tracks end up having large impact parameters in the Level-1 algorithm will be addressed in this Section. For the sake of clarity, we will focus on tracks with well-measured high-$p_T$ (good $p_T$ category) and defer the complete analysis for the other $p_T$ categories to the appendix.

Note that in the TDR Level-1 algorithm, the final decision criterion in principle involved another cut based on impact parameter significance (IPS), in conjunction with $p_T$, to guard against degradations in tracking performance [1]. For the tracking performance achieved for the TDR studies under normal conditions, the IPS component of the cut turned out to be largely irrelevant (see Fig. 7.3 in Ref. [1]), and we therefore ignore it in this study.

## 5.1 Single and multiple primary vertices at Level-1

An obvious reason for wrong IP assignment is the presence of multiple primary vertices. Before further investigating this issue, we should remind ourselves that the Level-1 algorithm, as used for the trigger and reoptimization TDR studies, was not designed to deal with events containing multiple primary vertices. The development of the Level-1 algorithms was based on the assumption that the Level-0 pile-up veto would remove events with multiple primary vertices for the most part. It was only with the studies performed in view of the trigger and reoptimization TDRs that the physics potential of pile-up events was explored in earnest. These studies showed that too stringent a pile-up veto (the default at the time was to cut at a multiplicity of 2 for the pile-up vertex) would severely diminish the yield of useful signal events. Factoring in considerations with respect to data size and processing time, a compromise was found, consisting of a pile-up vertex multiplicity cut at 3 in

conjunction with several hit multiplicity cuts (pile-up system and Scintillator Pad Detector, SPD).

An additional, considerable source of pile-up events is due to the Level-0 decision logic. It overrules the veto of the pile-up system (i.e. passes the event on to Level-1) in the presence of a dimuon sub-trigger. With the rather loose definition of dimuon at Level-0 (the sum of the two highest Level-0 muon transverse momenta above a threshold of 1.3 GeV, regardless of whether there is a second muon), this results in a rather large number of pile-up events to deal with at Level-1.

The upshot of all this was that the Level-1 algorithm was confronted with more pile-up events than initially foreseen. Within the time constraints of the TDR release there was no opportunity to address the problem, which, therefore remained an obvious short-coming of the Level-1 trigger design at the time of the TDR.

In the meantime, methods have been developed to cope with events containing multiple primary vertices at Level-1, see for instance Ref. [7].

## 5.2 IP categories

Similar to the $p_T$ assortment, we want to classify the tracks according to reasons behind false or correct IP assignments.

For the reasons detailed above, we will divide the sample into events with single and multiple primary vertices, where a primary vertex is only counted if it is *visible* in the detector. Here an interaction is said to be visible if it produces at least two charged particles with sufficient hits to allow them to be reconstructed as VELO tracks, i.e. not considering the information from the three tracking stations T1–T3 that are not available at the Level-1 stage.

For events with only one (visible) primary vertex, we may further divide the tracks according to their true IP as generated in the MC simulation (IPMC). We distinguish between tracks with true zero IP (IPMC $= 0$) and tracks with true non-zero IP (IPMC $> 0$). The latter category will comprise the tracks from bottom and charm decays.

In the case of multiple primary vertices the distinction according to true IP is not meaningful as we do not know a priori with respect to which vertex the IP should be evaluated. Therefore not much remains to be scrutinized in these events. The only interesting question in this case is whether we had a chance to detect the presence of multiple primary vertices and flag the event as such. We therefore divide the sample of events containing multiple primary vertices into events that have been vetoed by the pile-up system (but subsequently recovered by the dimuon sub-trigger) and events where the pile-up went unnoticed at Level-0.

We summarize the four categories we will use to classify decision tracks according to their cause for large IP:

- The decision track is part of an event with a single (visible) primary vertex:
  - **Single-PV, IPMC $= 0$** category: the track has a fake large IP;
  - **Single-PV, IPMC $> 0$** category: the track has a true large IP;

- The decision track is part of an event containing multiple (visible) primary vertices:
  - **Multiple-PV, PU = 0** category: the event is not flagged by the pile-up system;
  - **Multiple-PV, PU = 1** category: the event is flagged by the pile-up system ("dimuon leak").

If we assume that the problem of multiple primary vertices can be solved or at least ameliorated in future versions of the Level-1 algorithm and that the tracks with true large IP are the ones signalling interesting physics, then the only category deserving a closer look is the one containing tracks with fake large IP in events with a single visible primary vertex. In Subsection 5.4 we will further investigate this sample and try to find reasons for the wrong IP assignments in this case.

## 5.3 Decision tracks breakdown according to IP

As mentioned before, we focus on the dominant good $p_T$ category for the analysis of IP. The breakdown for this category, using the categories defined in the previous Subsection, is given in Table 4 and Fig. 8. Also given in Table 4 are the compositions of the various IP categories in terms of the truth categories defined in Sec. 3.

The breakdowns for the other $p_T$ categories is left to the Appendix A (Tables 5 and 6) and as an over-all summary, the IP breakdown for all the $p_T$ categories normalized to all the decision tracks is shown in Fig. 12.

For the good $p_T$ category the result is that about 70% of the decision tracks are due to the presence of multiple primary vertices. In two thirds of these cases, this was detected by the pile-up system, but subsequently ignored due to the presence of a Level-0 dimuon. It should be noted, however, that a substantial fraction of $b$-hadron tracks is contained in this category. Thus clever methods will be required to suppress the majority of pile-up events while keeping the efficiency for $b$-hadron events high.

As for events with a single primary vertex, there is a narrow majority of tracks with true large IP. This sample indeed mainly consists of tracks from bottom and charm decay. While there are no direct primary tracks in this sample, as expected with the requirement on true large IP, there is a non-negligible fraction of tracks from light resonances. These tracks acquire non-zero true IP either through multiple scattering (resulting in large IPs) or due to the numerical treatment of resonances in the simulation software (resulting in very small IPs).

**Table** 4: Number of "good $p_T$" decision tracks $N$ in each of the IP categories, and further split into the truth categories of Sec. 3. The fractions $F$ in the "All" row are normalized to all tracks in the respective primary-vertex class, the fractions given for the truth categories $A$, $B$, $C$, and $R$ are normalized to the respective IP categories. The uncertainties are statistical.

| | **Single** visible primary vertex $N = 1903$, $F = (29.8 \pm 0.6)\%$ | | | | **Multiple** visible primary vertices $N = 4473$, $F = (70.2 \pm 0.6)\%$ | | | |
|---|---|---|---|---|---|---|---|---|
| | IPMC = 0 | | IPMC > 0 | | PU = 0 | | PU = 1 | |
| Cat. | $N$ | $F$ [%] | $N$ | $F$ [%] | $N$ | $F$ [%] | $N$ | $F$ [%] |
| All | 833 | 43.8 ± 1.1 | 1070 | 56.2 ± 1.1 | 1451 | 32.4 ± 0.7 | 3022 | 67.6 ± 0.7 |
| $A$ | 453 | 54.4 ± 1.8 | 169 | 15.8 ± 1.1 | 635 | 43.8 ± 1.3 | 1370 | 45.3 ± 0.9 |
| $B$ | 0 | 0.0 ± 0.0 | 483 | 45.1 ± 1.5 | 75 | 5.2 ± 0.6 | 141 | 4.7 ± 0.4 |
| $C$ | 325 | 39.0 ± 1.7 | 0 | 0.0 ± 0.0 | 575 | 39.6 ± 1.3 | 1161 | 38.4 ± 0.9 |
| $R$ | 55 | 6.6 ± 0.9 | 418 | 39.1 ± 1.5 | 166 | 11.4 ± 0.8 | 350 | 11.6 ± 0.6 |

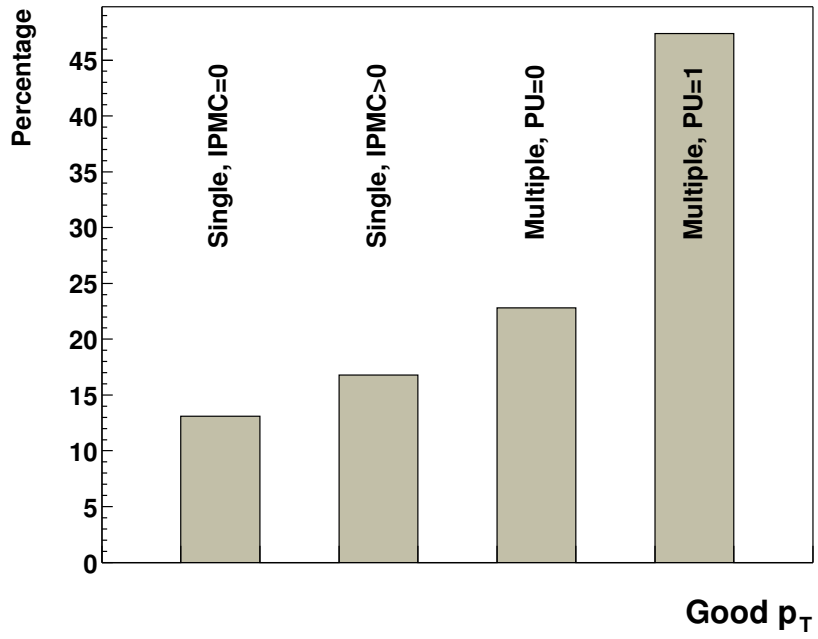


**Figure** 8: Graphical representation of the composition of the 6376 "good $p_T$" decision tracks according to the cause for large-IP

## 5.4 A closer look at the IP measurement in events with a single primary vertex

We now leave aside the case of multiple primary vertices and focus on the events with a unique visible primary vertex. Figures 9 and 10 show the (measured) IP distributions for the cases of zero and non-zero true IP, respectively, individually for the various truth categories of Sec. 3. While for IPMC = 0 the distributions are compatible with the fast falloff of some resolution effect, we clearly see for IPMC > 0 the effect of the bottom and charm lifetimes. The tracks from resonances (category *A*) contributing to IPMC > 0 feature a rather flat IP distribution, consistent with their being due to multiple scattering effects.

For comparison and completeness we add Fig. 11 showing the reconstructed IP distributions for events with multiple primary vertices. The IP is computed with respect to the "first" primary vertex, i.e. the one with the highest multiplicity. The large tail due to IP assignments obtained with the wrong primary vertex is clearly visible. We also see that the upper limit on IP removes a large fraction of such events, thus justifying this selection requirement.

The final and crucial point to be understood is why we trigger on tracks from the fake large IP category when the $p_T$ is well reconstructed. According to Table 4 we are left with 833 decision tracks in this category (good $p_T$, single-PV, IPMC = 0).

We have investigated two possible reasons for such erroneous IP assignments: the resolution of the primary vertex and the quality of the reconstructed Level-1 track.

Concerning the primary vertex quality, we observe very similar resolutions in $z$ of $\sigma_z \approx 40\,\mu$m for all truth categories. This means that the resolution of the primary vertex is the same for events containing $b$-hadrons and other events passing the Level-1 trigger. We may exclude it as the culprit for bad IP assignments.

As for track reconstruction quality, we have evaluated the mean $\chi^2$ of the track fit for the tracks in question. For the 453 tracks of category *A* we obtain $\langle\chi^2\rangle \approx 15$, for the 325 tracks of category *C* $\langle\chi^2\rangle \approx 16$. As a reference, we may use tracks from $b$-hadrons which have $\langle\chi^2\rangle \approx 8$. This is clear evidence that the fake large IPs are the result of badly reconstructed VELO tracks. A stronger requirement on the VELO track quality should be considered in future versions of the Level-1 algorithm.

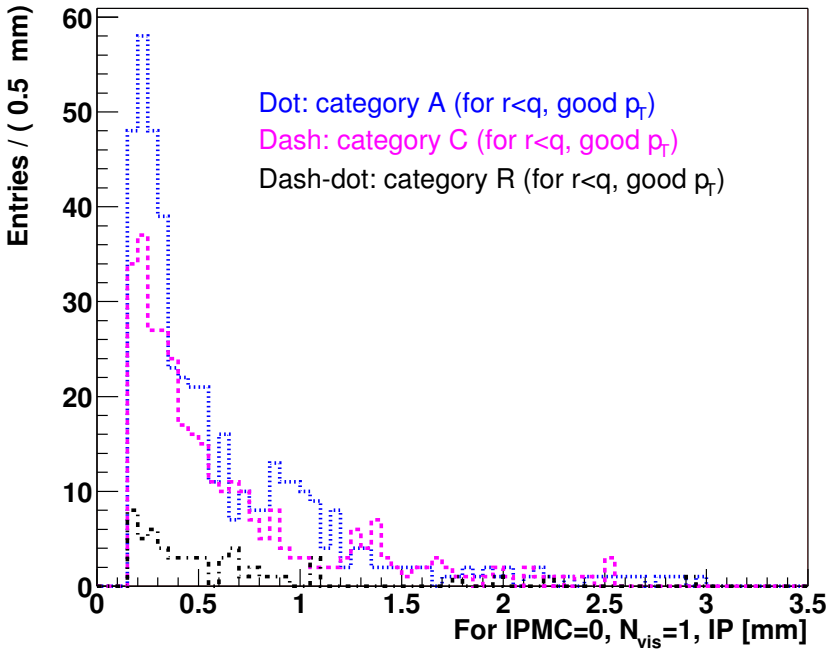


**Figure** 9: Reconstructed IP [mm], single primary and IPMC = 0 for the good $p_T$ category.

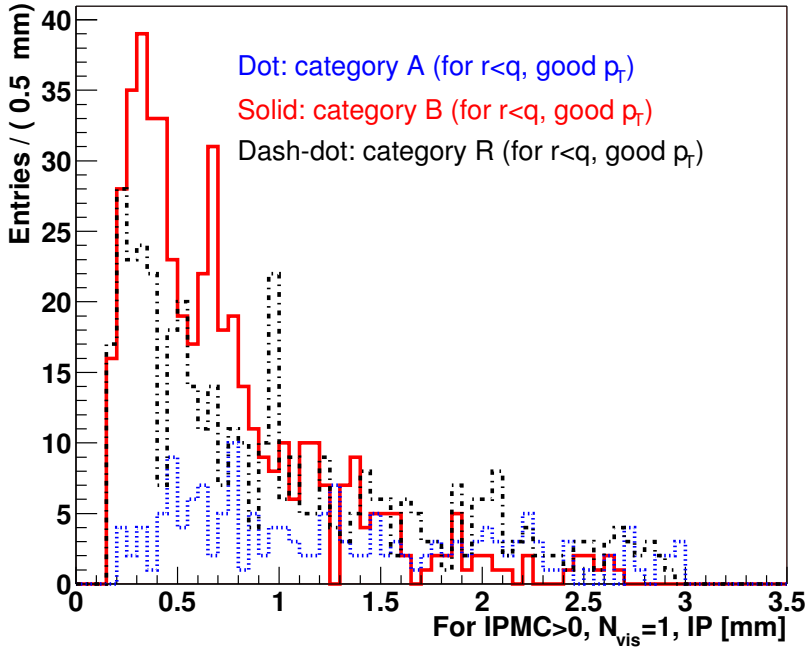


**Figure** 10: Reconstructed IP [mm], single primary and IPMC > 0 for the good $p_T$ category.

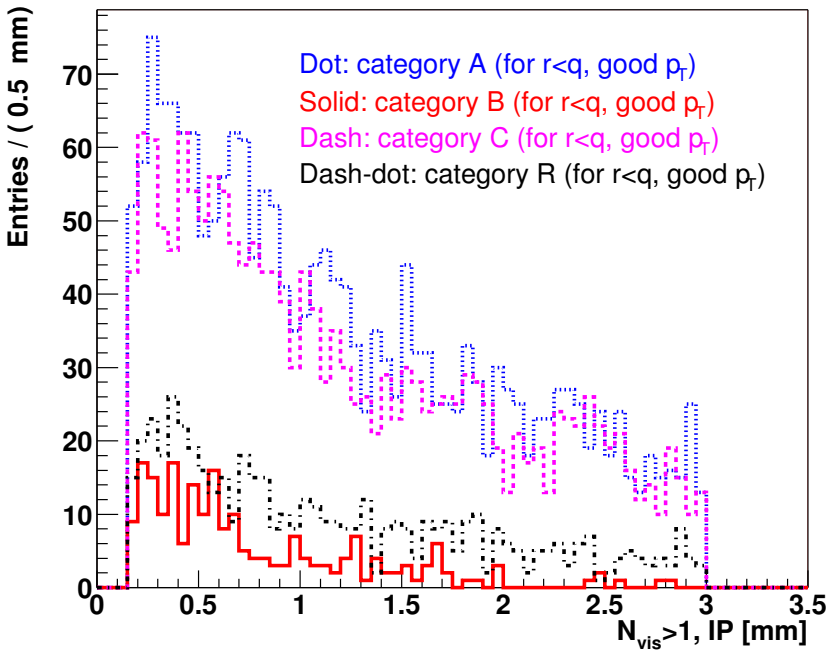


**Figure** 11: Reconstructed IP [mm], multiple primaries for the good $p_T$ category.

# 6 Conclusion and outlook

We summarize the main conclusions of our systematic analysis of the output of the generic Level-1 trigger:

- First of all, our study did not unearth any major shortcomings in our trigger strategy nor in the implementation (coding errors) other than the ones that are already known and are being addressed (such as the problem of multiple primary vertices).
- The $p_T$ part of the trigger works well: the large majority of tracks that trigger due to high-$p_T$ do so because they really do have high-$p_T$. The mistake rates due to bad resolution and wrong matching in the VELO–TT extrapolation process are found to be at levels that are to be expected with the precision available at Level-1 and account for bandwidth quotas of the order of 10% each.
- It is the IP part of the Level-1 algorithm that is responsible for filling most of the available bandwidth. By far the largest contribution is due to wrong IP assignments caused by the presence of multiple primary vertices in the same event. The problem is aggravated by the fact that the Level-0 pile-up veto is often overruled by a Level-0 dimuon signature, leading to a "dimuon" leak of pile-up events. Fortunately, this problem has already been addressed and appears to be under control in newer versions of the Level-1 software.
- Apart from the pile-up events, the main reason for large fake IPs appears to be due to a bad reconstruction quality of VELO tracks. This leads to bad extrapolation vectors back to the primary vertex, which are used for the IP determination.

Given that the main reason for minimum-bias triggers is to be looked for in the IP determination, we conclude that the most crucial variable parameter is the required minimum IP. A concurrent study on signal inefficiencies at Level-1 has come to the same conclusion [9], i.e. most of the useful signal events rejected at Level-1 are lost because of this cut. Instead of globally selecting all tracks above a certain minimum IP, a more flexible cut depending on global indicators of the event, the quality of the VELO track, or the measured $p_T$ could be envisaged. Of course any improvement in the quality of the track extrapolation back to the primary vertex would certainly help as well.

Many of these issues are already being addressed within the new trigger software framework developed for the 2004 data challenge (DC'04). Within the same framework, we plan to automate the track classification elaborated in this study and make it available in the form of a software tool. This means that in the future, the breakdowns according to trigger causes can be obtained automatically by switching on the corresponding option in the Level-1 trigger code.

In the long run, we should devise tools for understanding the composition of the trigger bandwidth without the use of Monte-Carlo truth in order to be prepared for real data taking in 2007 or 2008.

# A Decision tracks breakdown according to IP – other $p_T$ categories

Here we give the detailed breakdowns according to IP for the bad and wrong $p_T$ categories, Tables 5 and 6, respectively. In these cases, the fraction of events with multiple primary vertices is only about 60% whereas it is more than 70% in the good $p_T$ category. This significant difference comes from the fact that tracks with a spurious $p_T$ have a higher probability to be assigned a fake large IP as well, due to a generally worse track quality, thus increasing the fraction of single-primary events among the false triggers. The effect of the pile-up veto is independent of the $p_T$ category.

Turning to the events with single primary vertex, it is worth noting that decision tracks with bad and wrong $p_T$ mainly have vanishing true IPs, in contrast to tracks with good $p_T$, which are dominated by true non-zero IPs: The fact that the high $p_T$ is fake translates into a low probability for a track to come from a bottom or charm decay.

The breakdown for all the $p_T$ and IP categories normalized to all the decision tracks is graphically summarized in Figure 12.

**Table** 5: Number of "bad $p_T$" decision tracks $N$ in each of the IP categories, and further split into the truth categories of Sec. 3. The fractions $F$ in the "All" row are normalized to all tracks in the respective primary-vertex class, the fractions given for the truth categories $A$, $B$, $C$, and $R$ are normalized to the respective IP categories. The uncertainties are statistical.

| | **Single** visible primary vertex $N = 551$, $F = (41.6 \pm 1.4)\%$ | | | | **Multiple** visible primary vertices $N = 773$, $F = (58.4 \pm 1.4)\%$ | | | |
|---|---|---|---|---|---|---|---|---|
| | IPMC $= 0$ | | IPMC $> 0$ | | PU $= 0$ | | PU $= 1$ | |
| Cat. | $N$ | $F$ [%] | $N$ | $F$ [%] | $N$ | $F$ [%] | $N$ | $F$ [%] |
| All | 381 | $69.1 \pm 2.0$ | 170 | $30.9 \pm 2.0$ | 234 | $30.3 \pm 1.7$ | 539 | $69.7 \pm 1.7$ |
| $A$ | 206 | $54.1 \pm 2.6$ | 48 | $28.2 \pm 3.5$ | 120 | $51.3 \pm 3.3$ | 263 | $48.8 \pm 2.2$ |
| $B$ | 0 | $0.0 \pm 0.0$ | 26 | $15.3 \pm 2.8$ | 1 | $0.4 \pm 0.4$ | 8 | $1.5 \pm 0.5$ |
| $C$ | 150 | $39.4 \pm 2.5$ | 0 | $0.0 \pm 0.0$ | 85 | $36.3 \pm 3.1$ | 202 | $37.5 \pm 2.1$ |
| $R$ | 25 | $6.5 \pm 1.3$ | 96 | $56.5 \pm 3.8$ | 28 | $12.0 \pm 2.1$ | 66 | $12.2 \pm 1.4$ |

**Table** 6: Number of "wrong $p_T$" decision tracks $N$ in each of the IP categories, and further split into the truth categories of Sec. 3. The fractions $F$ in the "All" row are normalized to all tracks in the respective primary-vertex class, the fractions given for the truth categories $A$, $B$, $C$, and $R$ are normalized to the respective IP categories. The uncertainties are statistical.

| | **Single** visible primary vertex $N = 424$, $F = (40.8 \pm 1.5)\%$ | | | | **Multiple** visible primary vertices $N = 614$, $F = (59.2 \pm 1.5)\%$ | | | |
|---|---|---|---|---|---|---|---|---|
| | IPMC $= 0$ | | IPMC $> 0$ | | PU $= 0$ | | PU $= 1$ | |
| Cat. | $N$ | $F$ [%] | $N$ | $F$ [%] | $N$ | $F$ [%] | $N$ | $F$ [%] |
| All | 226 | $53.3 \pm 2.4$ | 198 | $46.7 \pm 2.4$ | 168 | $27.4 \pm 1.8$ | 446 | $72.6 \pm 1.8$ |
| $A$ | 160 | $70.8 \pm 3.0$ | 94 | $47.5 \pm 3.6$ | 115 | $68.5 \pm 3.6$ | 291 | $65.3 \pm 2.3$ |
| $B$ | 0 | $0.0 \pm 0.0$ | 18 | $9.1 \pm 2.0$ | 1 | $0.6 \pm 0.6$ | 6 | $1.3 \pm 0.6$ |
| $C$ | 43 | $19.0 \pm 2.6$ | 0 | $0.0 \pm 0.0$ | 21 | $12.5 \pm 2.6$ | 69 | $15.5 \pm 1.7$ |
| $R$ | 23 | $10.2 \pm 2.0$ | 86 | $43.4 \pm 3.5$ | 31 | $18.4 \pm 3.0$ | 80 | $17.9 \pm 1.8$ |

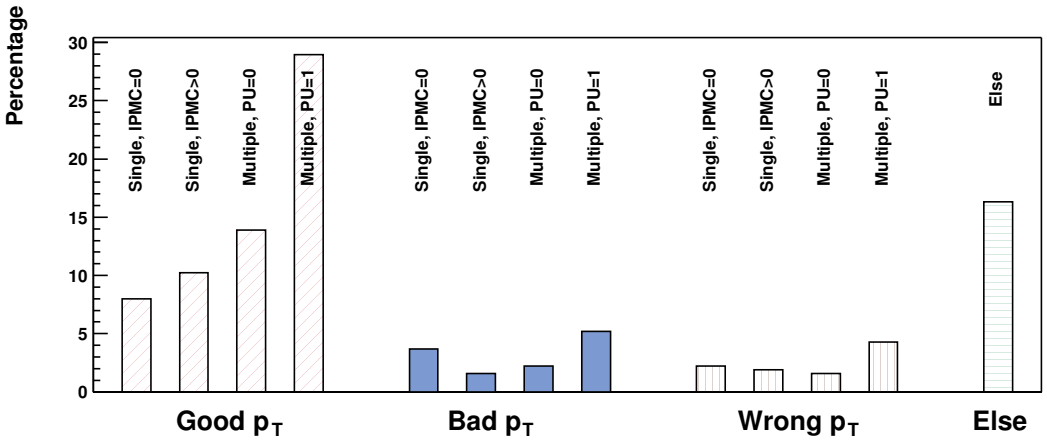


**Figure** 12: IP breakdown for all the $p_T$ categories; hatch (red): good $p_T$, solid (blue): bad $p_T$, vertical (brown): wrong $p_T$, horizontal (green): else.

# B Accumulation of pile-up events by generic and specific Level-1 algorithms

In a supplementary study we have compared the occurrence of pile-up events and the corresponding pile-up veto response for the sample triggered by the generic part of Level-1 with that for the sample triggered by the specific algorithms[3] (bonus system). The result is summarized in Table 7.

As expected, the fraction of pile-up events is significantly lower in the sample triggered by the specific algorithm. This is another manifestation of the fact that the generic algorithm, in its TDR incarnation, accumulates pile-up events because of the IP requirement. The efficiency of the pile-up veto is the same for both classes of events.

**Table** 7: Comparison of the fraction of pile-up events in the samples triggered by the generic and specific algorithms of Level-1. The uncertainties on the fractions are statistical.

**Generic algorithm**: 5220 events, $(72.6 \pm 0.5)\%$

| $N_{\rm vis} = 1$ | $F_{N_{\rm vis}=1}$ [%] | $N_{\rm vis} > 1$ | $F_{N_{\rm vis}>1}$ [%] |
|---|---|---|---|
| 1953 | $37.4 \pm 0.7$ | 3267 | $62.6 \pm 0.7$ |

| Pile-Up Veto Decision ($N_{\rm vis} > 1$) | | | |
|---|---|---|---|
| PU = 0 | $F_{\rm PU=0}$ [%] | PU = 1 | $F_{\rm PU=1}$ [%] |
| 1037 | $31.7 \pm 0.8$ | 2230 | $68.3 \pm 0.8$ |

**Specific algorithm**: 1971 events, $(27.4 \pm 0.5)\%$

| $N_{\rm vis} = 1$ | $F_{N_{\rm vis}=1}$ [%] | $N_{\rm vis} > 1$ | $F_{N_{\rm vis}>1}$ [%] |
|---|---|---|---|
| 1129 | $57.3 \pm 1.1$ | 842 | $42.7 \pm 1.1$ |

| Pile-Up Veto Decision ($N_{\rm vis} > 1$) | | | |
|---|---|---|---|
| PU = 0 | $F_{\rm PU=0}$ [%] | PU = 1 | $F_{\rm PU=1}$ [%] |
| 285 | $33.8 \pm 1.6$ | 557 | $66.2 \pm 1.6$ |

[3]Note that events labeled as triggered by the specific algorithms are those that would not have been triggered by the generic algorithm alone. Thus, they may in fact have been triggered by a combination of generic and specific algorithms.

# References


[1] Antunes Nobrega, R. *et al.* (LHCb collaboration), *LHCb Trigger System Technical Design Report*, CERN/LHCC 2003–031, LHCb TDR 10, September 2003.

[2] Jacoby, C. and Schietinger, T., *Level-1 decision algorithm and bandwidth division*, LHCb/2003–111 TRIG.

[3] Witek, M., *VELO–TT matching and momentum determination at Level-1 trigger*, LHCb/2003–060 TRIG.

[4] Dijkstra, H. *et al.*, *The use of the TT1 tracking station in the Level-1 trigger*, LHCb/2002–045 TRIG.

[5] Antunes Nobrega, R. *et al.* (LHCb collaboration), *LHCb Reoptimized Detector (Design and Performance) Technical Design Report*, CERN/LHCC 2003–030, LHCb TDR 9, September 2003.

[6] Witek, M., private communication.

[7] Witek, M., *Improvements in the L1 algorithm – post TDR status and plans*, talk given at the Nov. 2003 LHCb week (26 November 2003), `http://agenda.cern.ch/askArchive.php?base=agenda&categ=a035951&id=a035951s1t0/transparencies`.

[8] Ferro-Luzzi, M., *Effect of multiplicity cuts on the L0 and L1 triggers*, LHCb/2003–047.

[9] Legger, F. and Schietinger T., *B tracks in signal events rejected by the Level-1 trigger*, LHCb/2004–046 TRIG.